Systems/Circuits

A Corticocortical Circuit Directly Links Retrosplenial Cortex to M2 in the Mouse

Naoki Yamawaki,[1] Jelena Radulovic,[2] and Gordon M.G. Shepherd[1]

[1]Department of Physiology and [2]Department of Psychology, Feinberg School of Medicine, Northwestern University, Chicago, Illinois 60611

Retrosplenial cortex (RSC) is a dorsomedial parietal area involved in a range of cognitive functions, including episodic memory, navigation, and spatial memory. Anatomically, the RSC receives inputs from dorsal hippocampal networks and in turn projects to medial neocortical areas. A particularly prominent projection extends rostrally to the posterior secondary motor cortex (M2), suggesting a functional corticocortical link from the RSC to M2 and thus a bridge between hippocampal and neocortical networks involved in mnemonic and sensorimotor aspects of navigation. We investigated the cellular connectivity in this RSC→M2 projection in the mouse using optogenetic photostimulation, retrograde labeling, and electrophysiology. Axons from RSC formed monosynaptic excitatory connections onto M2 pyramidal neurons across layers and projection classes, including corticocortical/intratelencephalic neurons (reciprocally and callosally projecting) in layers 2–6, pyramidal tract neurons (corticocollicular, corticopontine) in layer 5B, and, to a lesser extent, corticothalamic neurons in layer 6. In addition to these direct connections, disynaptic connections were made via posterior parietal cortex (RSC→PPC→M2) and anteromedial thalamus (RSC→AM→M2). In the reverse direction, axons from M2 monosynaptically excited M2-projecting corticocortical neurons in the RSC, especially in the superficial layers of the dysgranular region. These findings establish an excitatory RSC→M2 corticocortical circuit that engages diverse types of excitatory projection neurons in the downstream area, suggesting a basis for direct communication from dorsal hippocampal networks involved in spatial memory and navigation to neocortical networks involved in diverse aspects of sensorimotor integration and motor control.

Key words: **circuit; motor; neocortex; optogenetic; retrosplenial**

Significance Statement

Corticocortical pathways interconnect cortical areas extensively, but the cellular connectivity in these pathways remains largely uncharacterized. Here, we show that a posterior part of secondary motor cortex receives corticocortical axons from the rostral retrosplenial cortex (RSC) and these form monosynaptic excitatory connections onto a wide spectrum of excitatory projection neurons in this area. Our results define a cellular basis for direct communication from RSC to this medial frontal area, suggesting a direct link from dorsal hippocampal networks involved in spatial cognition and navigation (the "map") to sensorimotor networks involved the control of movement (the "motor").

Introduction

Retrosplenial cortex (RSC) is a dorsomedial parietal area involved in diverse cognitive functions, including spatial navigation, orienting, memory, and planning (Epstein, 2008; Vann et al., 2009; Aggleton, 2014; Miller et al., 2014). Anatomically, the RSC receives diverse axons from dorsal hippocampus and parahippocampal areas and sends axons to various cortical areas (Sugar et al., 2011), suggesting that the RSC is hodologically organized to convey information from dorsal hippocampal to neocortical networks (Cho and Sharp, 2001; Whitlock et al., 2008; Vann et al., 2009; Sugar et al., 2011). However, the cellular circuits mediating this hippocampal→RSC→neocortical communication remain largely uncharacterized.

Anatomical studies in rats indicate that a major cortical target of RSC axons, particularly those arising from the more anterior part of the RSC, is a region directly anterior to the RSC in the posteromedial frontal cortex (Vogt and Miller, 1983; Van Groen and Wyss, 2003; Shibata et al., 2004; Sugar et al., 2011; Hooks et al., 2013; Vogt and Paxinos, 2014). The mouse homolog of this rostral projection of the RSC, though not previously characterized in detail, appears similarly organized based on the available

Received April 2, 2016; revised July 21, 2016; accepted July 24, 2016.

Author contributions: N.Y., J.R., and G.M.G.S. designed research; N.Y. performed research; N.Y. analyzed data; N.Y., J.R., and G.M.G.S. wrote the paper.

This work was supported by the National Institute of Neurological Disorders and Stroke–National Institutes of Health (Grant NS061963) and the National Institute of Mental Health–National Institutes of Health (Grant MH108837). We thank K. Guo and B. Suter for advice and suggestions and C. Maguire for technical assistance.

The authors declare no competing financial interests.

Correspondence should be addressed to either Naoki Yamawaki or Gordon M.G. Shepherd, Department of Physiology, Feinberg School of Medicine, Northwestern University, Morton 5-660, 303 E. Chicago Ave., Chicago, IL 60611. E-mail: yamawakn@gmail.com or gmgshepherd@gmail.com.

DOI:10.1523/JNEUROSCI.1099-16.2016

 0270-6474/16/369365-10$15.00/0

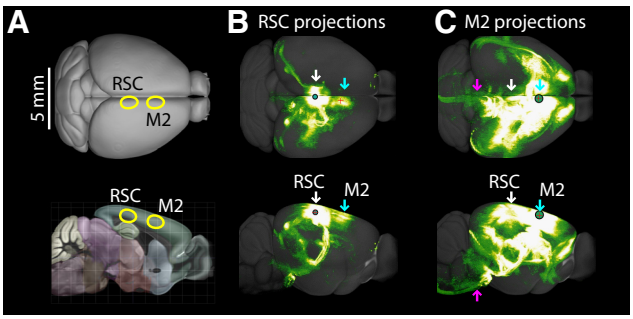

Figure 1. Allen Mouse Brain Connectivity Atlas images suggest an anatomical basis for RSC corticocortical connections to posterior M2. ***A***, Dorsal (top row) and sagittal (bottom row) views of the mouse brain indicating the locations of the RSC and M2 areas examined in this study. ***B***, Injection in the RSC (white arrow) shows a corticocortical projection to M2 in the posteromedial frontal cortex (cyan arrow). ***C***, Injection in the M2 (cyan arrow), corresponding to the RSC-recipient zone, shows projections to diverse regions including back to the RSC (white arrow) and subcortical regions such as the pyramidal tract (magenta arrow). Images are maximum intensity projections that were viewed, copied, and modified from experiments 100148142 (RSC injection) and 180916954 (M2 injection) of the Allen Mouse Brain Connectivity Atlas.

data in the Allen Mouse Brain Connectivity Atlas (available at http://connectivity.brain-map.org/; 2014 Allen Institute for Brain Science; Oh et al., 2014), which defines the area receiving these RSC axons as a posterior part of secondary motor (M2) area (Fig. 1*A–C*). The behavioral functions of this area are not well understood. Microstimulation in and around this region can evoke movements of the neck, tongue, face, eyes, vibrissae, and other upper-body muscles (Li and Waters, 1991; Brecht et al., 2004; Tandon et al., 2008; Komiyama et al., 2010; Tennant et al., 2011; Hooks et al., 2011; Smith and Alloway, 2013; Hollis et al., 2016). Inactivation studies, however, suggest roles in attention and choice-based behaviors (Passetti et al., 2002; Koike et al., 2016). Anatomically, this posterior part of M2 appears to project prodigiously and divergently throughout much of the CNS, including interhemispheric, pyramidal tract, and many other branches (Fig. 1*C*). The RSC→M2 projection has been hypothesized to enable RSC neurons to communicate with frontal neurons involved in sensorimotor integration and motor control (Vogt and Miller, 1983; Shibata et al., 2004), but the cellular targets of RSC axons in the M2, and thus the specific circuit connections mediating this communication, have not been identified.

Indeed, it has been emphasized that whereas the extensive anatomical data constitute a detailed retrosplenial connectome, information is notably lacking about functional connectivity in these circuits (Sugar et al., 2011). Evaluating RSC→M2 synaptic connectivity at the level of identified cell types is thus an important step toward understanding the mechanistic basis for communication along the dorsal edge of the hippocampal–neocortical network. By combining optogenetics, retrograde labeling, and *ex vivo* whole-cell recording, we functionally dissected the cell-type-specific excitatory synaptic connectivity constituting the RSC→M2 circuit in the mouse.

Materials and Methods

Studies were approved by the Northwestern University Animal Care and Use Committee and followed the animal welfare guidelines of the Society for Neuroscience and the National Institutes of Health. Wild-type mice (C57BL/6, female and male) were bred in-house or purchased from Jackson Laboratory. Mice were 6–9 weeks old at the time of brain slice recordings.

The experimental approach, based on *in vivo* stereotaxic injections followed by *in vitro* photostimulation of presynaptic axons expressing channelrhodopsin-2 (ChR2; Petreanu et al., 2007; Petreanu et al., 2009) and postsynaptic single-cell electrophysiological recordings from identified pyramidal neurons in brain slices, has been described in detail in recent studies (Suter and Shepherd, 2015; Yamawaki and Shepherd, 2015; Yamawaki et al., 2016).

After preparation of brain slices, the slices containing the injection site were carefully inspected to verify the accuracy of the stereotaxic targeting and to ensure that labeling was focal and restricted to the region of interest (RSC or M2). Injections in the RSC labeled neurons in both the granular (RSCg) and dysgranular (RSCd) regions. Pharmacological conditions were set to isolate monosynaptic photo-evoked inputs, including tetrodotoxin (TTX) and 4-aminopyridine (4AP) in the bath solution (artificial CSF, ACSF; Petreanu et al., 2009), and NMDA receptors were blocked with CPP (5 μM). Recordings were made in ACSF composed of the following (in mM): 127 NaCl, 25 $NaHCO_3$, 25 D-glucose, 2.5 KCl, 1 $MgCl_2$, 2 $CaCl_2$, and 1.25 NaH_2PO_3. Recordings were made at 22°C. Borosilicate electrodes for whole-cell recordings were filled with internal solution composed of the following (in mM): 128 potassium methanesulfonate, 10 HEPES, 10 phosphocreatine, 4 $MgCl_2$, 4 ATP, 0.4 GTP, 3 ascorbate, and 1 EGTA, pH 7.25, 290–295 mOsm.

For photostimulation experiments, we used a light-emitting diode (LED; M470L2; Thorlabs) mounted in the epifluorescence pathway of an upright microscope (Olympus BX51 chassis) equipped with a low-magnification objective lens (4×, UPlanSApo, numerical aperture 0.16; Olympus) to generate photostimuli consisting of a single wide-field blue flash (duration 5 ms; intensity 1.27 mW/mm^2 in the specimen plane). For each neuron, single-pulse photostimulation trials were repeated three or more times, traces were averaged, and the average current amplitude over the time window 0–50 ms after stimulus was calculated and used to represent that neuron's photo-evoked synaptic input (Yamawaki and Shepherd, 2015). Recordings were sequentially targeted to neighboring pairs of projection neurons ($<$100 μm) that were identified as different projection neurons based on labeling with different colored tracers. In some cases, a nearby third neuron was also recorded, allowing two pairwise comparisons from three projection neurons.

Data acquisition and hardware settings for photostimulation and electrophysiology were controlled by Ephus version 2.1.0 software (Suter et al., 2010; www.ephus.org).

For statistical analyses, group data are presented as median unless otherwise indicated and group comparisons were made using nonparametric tests as indicated in the text, with significance defined as $p < 0.05$.

Three-dimensional views of the mouse brain and maximum intensity projection images for injection sites corresponding most closely to the RSC and M2 areas studied here were obtained from the Allen Mouse Brain Connectivity Atlas.

Results

RSC axons project to posterior M2

Most previous studies of the anatomy of the RSC→M2 projection in rodents have used rats (Vogt and Miller, 1983; Shibata et al., 2004). Images from the Allen Mouse Brain Connectivity Atlas suggest similar anatomical organization in mice (Fig. 1*A*). Building on these observations and as an initial step toward characterizing RSC→M2 synaptic connections in the present study, we used retrograde and anterograde labeling methods to localize the RSC→M2 projection anatomically in mice. In one set of experiments, we injected retrograde tracer into the M2 and, several days later, prepared RSC-containing coronal brain slices (Fig. 2*A*). Fluorescent retrogradely labeled M2-projecting neurons were observed in the RSC, mostly in the upper layers (Fig. 2*A*). Later in the study we will describe additional details of this labeling pattern. In a complementary set of experiments, we injected anterograde marker (AAV-eGFP) into the RSC and prepared coronal M2-containing slices 3 weeks later (Fig. 2*B–E*). Fluorescent RSC axons were observed in a wedge-like sector extending dorsomedially along the flexure between the lateral agranular cortex and the medial bank within the interhemispheric fissure (Fig. 2*D*,*E*). In stereotaxic atlases, this RSC-recipient zone corresponds to the

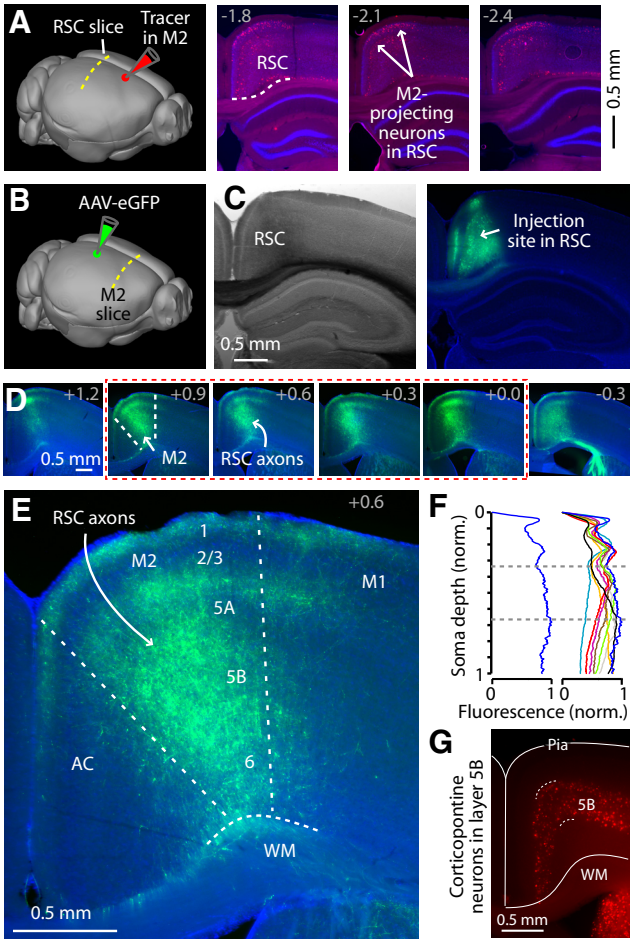

Figure 2. RSC axons project to posterior M2. ***A***, Left, Retrograde tracer injection into the M2 to identify M2-projecting neurons in RSC brain slices. Right, Rostrocaudal series of epifluorescence images showing labeling of M2-projecting neurons (red) in the RSC. Distance from bregma is indicated at the top right. Blue, DAPI staining. Arrows, M2-projecting neurons located in the upper layers of the RSC. ***B***, Schematic showing injection of AAV-eGFP into the RSC for anterograde labeling of RSC axons in M2. ***C***, Bright-field (left) and epifluorescence (right) images of an RSC injection site (green). Blue, DAPI staining. ***D***, Rostrocaudal series of epifluorescence images showing labeling of RSC axons in the M2. Labeling is densest at the cortical flexure, where lateral agranular cortex curves medially into the interhemispheric fissure. Numbers in each image indicate the distance from bregma. Red rectangle indicates range of slices used for recording. Blue, DAPI staining. ***E***, Enlargement of the third image in ***E*** with cortical layers indicated. WM, White matter. M1 is laterally adjacent to the M2 and the anterior cingulate (AC) is medially adjacent. ***F***, Normalized fluorescent intensity across layers, for the slice in ***E*** (left) and for a total of nine slices (right). Dashed lines indicate layer 5B. ***G***, Layer 5B in M2 (between dashed lines) defined by retrogradely labeled corticopontine neurons. Layer 5B is a relatively thick layer in M2, spanning approximately the middle third of the cortex.

posterior part of M2 (Dong, 2008). The RSC axonal projection to M2 extended 1–2 mm along the rostrocaudal axis. Guided by these anterograde and retrograde labeling patterns, in subsequent experiments of RSC→M2 connections we targeted our injections and recordings to an RSC location of −1.4 mm and a M2 location of +0.5 mm rostrocaudal distance relative to bregma. In M2 slices at this level (Fig. 2*E*), RSC axons extended across M2 layers, with relative peaks in upper layer 1, lower 2/3, and broadly across 5B/6 (Fig. 2*F*). Layer 5B is particularly thick in the M2 (Fig. 2*G*; Hooks et al., 2011), as expected for a cortical area at the crest of a convexity (von Economo, 1929). This anatomical distribution suggested that M2 neurons across layers could be broadly innervated by these RSC axons, which we tested next.

RSC axons monosynaptically excite pyramidal neurons across multiple layers in M2

To assess synaptic connectivity in these RSC→M2 projections, we used a strategy based on photostimulation of ChR2-expressing presynaptic axons while recording from identified postsynaptic neurons in the downstream area of interest (see Materials and Methods). Among several key advantages of this ChR2-based method for cell-type-specific electro-anatomical analysis of synaptic connections are its high sensitivity for detecting connections due to high release probability at photostimulated terminals, its high specificity for activating inputs from presynaptic sources of interest while avoiding axons of passage, and its ability to isolate purely monosynaptic inputs (Schoenenberger et al., 2011; Yamawaki et al., 2016). We injected the RSC with AAV-ChR2-Venus and prepared coronal brain slices containing the M2 ~3 weeks later (Fig. 3*A–C*). Whole-cell recordings were made from neurons with pyramid-like somata located at various depths from the pia (Fig. 3*D*), measured as absolute (in millimeters) and normalized (pia = 0, and white matter = 1) distances. For each neuron, brief pulses of blue light from an LED were delivered through a low-magnification objective lens while recording responses in voltage-clamp mode, with TTX and 4-AP present in the bath solution to eliminate polysynaptic activity and thereby isolate monosynaptic excitatory inputs from presynaptic terminals directly connected to the recorded neuron (see Materials and Methods; Petreanu et al., 2009). This process was repeated for multiple radially aligned neurons per slice (Fig. 3*E*). For each slice, a laminar profile was generated by plotting the collection of response amplitudes against the soma depths, normalizing to the maximum value. Laminar profiles were obtained from multiple slices and the data were pooled (4–9 neurons/profile; 1 profile/slice; 8 slices from $n = 6$ animals; Fig. 3*F*,*G*). These results indicated that essentially all neurons received detectable excitatory input, but response amplitudes were variable, with generally stronger responses in the upper and middle levels of the cortex, corresponding to layers 2/3–5A and 5B, respectively, and weaker responses in the deepest third, corresponding to layer 6 (Fig. 3*G*).

RSC axons excite diverse projection neurons in M2

Cortical pyramidal neurons can be classified, not only by laminar location, but also by long-range axonal projections, which follow distinct patterns (Harris and Shepherd, 2015) and can therefore be identified by retrograde labeling methods. We used these to assess the connections formed by RSC axons onto different types of projection neurons in M2.

Anatomically, the M2 projects back to the RSC (Fig. 1), so RSC input to the neurons forming this projection would constitute a recurrent functional circuit (RSC→M2→RSC). We therefore started by addressing whether RSC axons excite RSC-projecting corticocortical neurons in M2. We injected retrograde tracer (CTB647) and anterograde tracer (AAV-ChR2-Venus) into the RSC and prepared brain slices containing M2 (Fig. 4*A*,*B*), similar to previous approaches used to examine other recurrent connections (Mao et al., 2011; Little and Carter, 2013; Suter and Shepherd, 2015; Yamawaki and Shepherd, 2015). We recorded from RSC-projecting neurons in layer 2/3 and layer 5B, where unlabeled neurons were found to receive strong RSC input in the preceding experiment (Fig. 3*G*). Photostimulation of RSC axons evoked excitatory synaptic currents in RSC-projecting neurons in both layers that were similar in amplitude (median ratio of responses in layer 2/3 versus 5B neurons: 1.16; $p = 0.68$, sign test; $n = 6$ layer 2/3 and 4 layer 5B neurons recorded in 4

slices from $n = 3$ animals, yielding 6 pairwise comparisons; Fig. 4*C*,*D*), similar to the laminar analysis (Fig. 3*G*). This demonstrates a recurrent pattern of connectivity insofar as RSC axons in the M2 excited RSC-projecting neurons. The recurrent connectivity at the RSC end of the circuit will also be addressed later.

Next, we undertook a series of experiments using RSC-projecting neurons as a basis for comparison with projection neurons of another class located nearby (within 0.1 mm) at the same laminar level. We started with layer 6, which contains a mix of corticothalamic (CT) and intratelencephalic (IT) neurons (Harris and Shepherd, 2015; Yamawaki and Shepherd, 2015). Retrograde tracers of different colors were injected in the ventrolateral nucleus and the RSC and AAV-ChR2-Venus was injected in the RSC (Fig. 4*E*). In M2 brain slices, recordings were made sequentially from fluorescently labeled CT neurons and neighboring RSC-projecting neurons in layer 6 (Fig. 4*F*,*G*). There was no overall difference in the amplitude of photo-evoked excitatory input from RSC axons to these CT and RSC-projecting neurons in M2 (median ratio of CT/RSC-projecting responses: 0.73; $p = 0.42$, sign test; $n = 14$ CT and 10 RSC-projecting neurons recorded in 10 slices from $n = 5$ animals, yielding 14 pairwise comparisons; Fig. 4*H*). Although the absolute response amplitudes were low compared with inputs to layer 2/3 and 5B neurons (measured in the previous experiments), they were readily detectable above noise levels, indicating that both cell types consistently received RSC input. The RSC innervation of both CT and IT neurons in M2 contrasts with long-range inputs to visual cortex, which innervate CT but not IT neurons in layer 6 (Vélez-Fort et al., 2014), indicating an areal difference in this aspect of corticocortical connectivity.

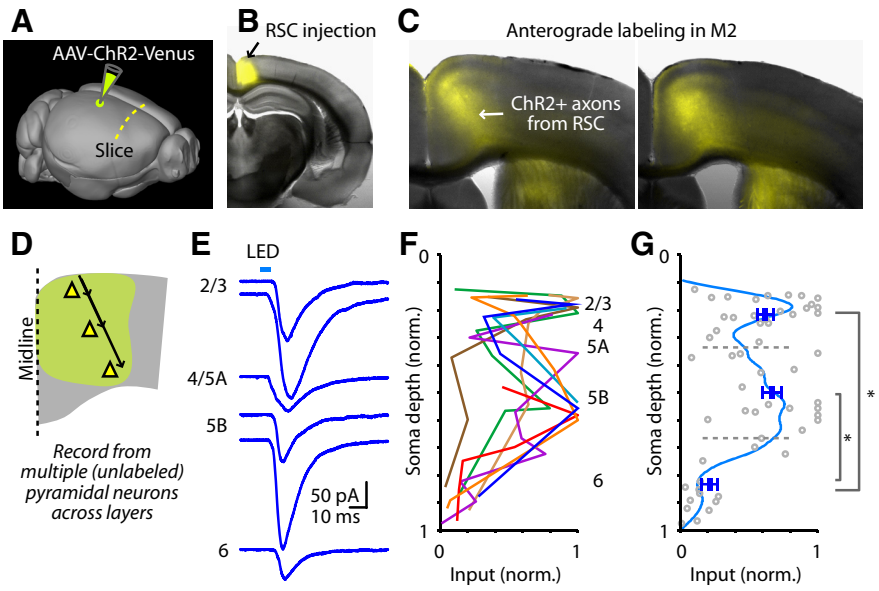

Figure 3. RSC axons monosynaptically excite pyramidal neurons across multiple layers in M2. ***A***, Schematic of the experimental paradigm, indicating injection of anterograde tracer (AAV-ChR2-Venus) into the RSC, resulting in anterograde labeling of RSC axons projecting to M2. ***B***, Low-magnification bright-field image merged with epifluorescence image showing the location of the RSC injection site. ***C***, Merged bright-field and epifluorescence images of brain slices containing the M2 and RSC axons over a range of rostrocaudal levels, similar to Figure 2, *D* and *E*. ***D***, Schematic of experimental paradigm: M2-projecting axons of RSC neurons were anterogradely labeled and M2 slices were subsequently prepared. In each slice, multiple M2 pyramidal neurons were recorded at different cortical depths along the same radial axis (arrows). ***E***, Example traces recorded from multiple neurons in the same slice. ***F***, Collection of laminar profiles from a different slice (indicated with different color). The blue profile is from the traces in ***E***. ***G***, Data from ***F*** are replotted (gray circles) and grouped by dividing the cortical depths into thirds (indicated by dashed lines), which corresponds approximately to layer 2 through 5A in the top third, layer 5B in the middle third, and layer 6 in the bottom third. Blue symbols represent the mean ± SEM for each group. Rank-sum tests for the three groups (significance defined as $p < 0.05/3 = 0.0167$ to correct for multiple comparisons) showed the following: top versus middle, $p = 0.44$; middle versus bottom, $p = 1.8e\text{-}04$; and top versus bottom, $p = 9.7e\text{-}05$. The data were fit with a polynomial function (light blue trace; generated with Matlab's cftool using the smoothing spline option with the smoothing parameter set to 0.999973).

We next considered layer 5B, which contains a mix of pyramidal tract (PT) and IT neurons (Anderson et al., 2010; Harris and Shepherd, 2015). PT neurons send axon branches to diverse subcortical regions generally associated with sensory and motor functions and can thus be labeled by injecting retrograde tracers into these areas. Accordingly, to label PT neurons in M2 we injected either the pontine nuclei to label corticopontine neurons (Fig. 4*I*,*J*) or the superior colliculus (Fig. 4*L*,*M*) to label corticocollicular neurons. In the same animals, we also injected another tracer into the RSC to label RSC-projecting neurons in the M2 with a different color. AAV-ChR2-Venus was also injected into the RSC. Recordings were made from monolabeled neurons to exclude PT neurons with RSC branches (which, however, appeared to be scarce, because double-labeled PT neurons were only infrequently observed). Responses showed no overall differences between either corticopontine (Fig. 4*K*,*L*) or corticocollicular (Fig. 4*O*,*P*) neurons compared with RSC-projecting neurons (median ratio of corticopontine/RSC-projecting responses: 0.75; $p = 0.30$, sign test; 12 corticopontine and 11 RSC-projecting neurons recorded in 7 slices from $n = 4$ animals, yielding 15 pairwise comparisons; for corticocollicular/RSC-projecting: 0.89; $p = 0.58$, sign test; 13 corticocollicular and 12 RSC-projecting neurons recorded in 8 slices from $n = 6$ animals, yielding 13 pairwise comparisons). In a separate set of experiments, we also recorded from another type of PT neuron, cervically projecting corticospinal neurons. These were found in scarce numbers in M2, but those that were present received strong RSC input; in contrast, those located laterally in M1, where these corticospinal neurons are highly abundant, received no detectable input (data not shown).

We further explored the RSC innervation of M2 projection neurons by injecting the contralateral M2 to label callosally projecting IT neurons; in the same animals, we also injected the RSC with both another tracer and with AAV-ChR2-Venus (Fig. 4*M*,*N*). Pairwise recordings from callosally projecting and RSC-projecting neurons both in layer 2/3 and in layer 5B showed no differences in excitatory input (median ratio of callosally projecting/RSC-projecting responses in layer 5B: 0.62; $p = 0.25$, sign test; 9 callosally projecting and 7 RSC-projecting neurons recorded in 7 slices from $n = 5$ animals, yielding 9 pairwise comparisons; for pairs in layer 2/3: 1.05; $p = 0.98$, sign test; 10 callosally projecting and 11 RSC-projecting neurons recorded in 7 slices from $n = 5$ animals, yielding 15 pairwise comparisons; Fig. 4*O*,*P*).

This series of experiments examining RSC synaptic connectivity to different types of projection neurons in M2 did not find evidence for preferential innervation of one class over another within the same layer. Instead, RSC axons broadly innervated M2 projection neurons, suggesting that the RSC→M2 circuit can

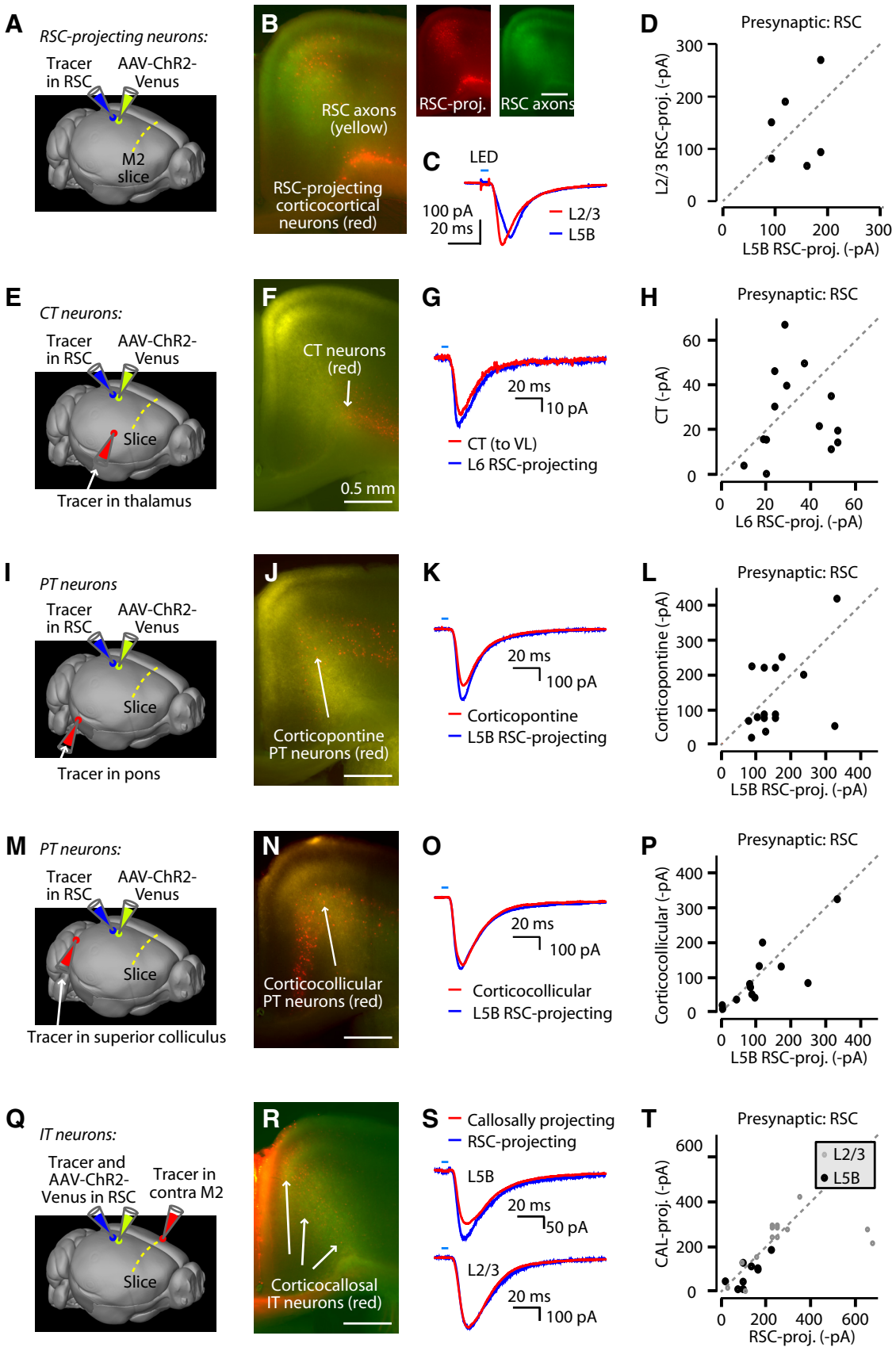

Figure 4. RSC axons excite diverse projection neurons in M2. ***A***, Schematic of the experimental paradigm: to assess RSC input to RSC-projecting neurons in M2, retrograde tracer (CTB647) and AAV-ChR2-Venus were injected into the RSC. ***B***, Left, Merged epifluorescence image of M2 slice containing RSC-projecting neurons (red) and RSC axons (yellow) in M2. Unmerged epifluorescence images are shown on the right. ***C***, Example traces of photo-evoked RSC input recorded from layer 2/3 (red) and layer 5B (blue) RSC-projecting neurons in M2. ***D***, Group comparison of RSC input to layer 2/3 and layer 5B RSC-projecting neurons (not significantly different; see Results). ***E***, Schematic of the experimental paradigm: to compare RSC input to CT neurons (*Figure legend continues.*)

directly (monosynaptically) influence a diverse array of outputs from the M2.

In all of our optogenetic-electrophysiology experiments, we strove for consistency in targeting the RSC injections and M2 recordings to the same anatomical locations in cortex. *Post hoc* morphometric analyses showed that the mean rostrocaudal locations of the injected and recorded slices were −1.4 and +0.5 mm (relative to bregma), respectively (Fig. 5*A*). Within the M2, recordings had been made within a narrow (~0.5 mm) columnar strip of cortex within the densest part of the RSC axonal projection (Fig. 5*B*). Therefore, from an anatomical standpoint, these data confirm that injections and recordings had been performed in a consistent and precise manner.

Disynaptic RSC connections to M2 via corticocortical and trans-thalamic circuits

The main focus of this study is on monosynaptic excitatory RSC→M2 connections because these constitute the most direct channels of communication in this pathway. However, we also considered disynaptic pathways, which could serve as additional (perhaps modulatory) pathways of communication. For this, we again injected the RSC with AAV-ChR2-Venus, but in this case, we targeted the retrograde tracer injections to the M2 (Fig. 6*A*). In subsequently prepared coronal slices, we then searched for brain regions where the anterogradely labeled RSC axons anatomically overlapped with retrogradely labeled M2-projecting neurons, focusing on cortex and thalamus (the two primary sources of long-range excitatory inputs to cortical areas).

In cortex, we identified prominent such overlap in the posterior parietal cortex (PPC; Fig. 6*B*). In PPC brain slices, we targeted the M2-projecting neurons for recordings and photostimulated the RSC axons (9 neurons recorded in 3 slices from $n = 3$ animals) and observed moderate-to-strong excitatory responses in most of these neurons (Fig. 6*C*). These findings thus demonstrate a circuit-level basis for disynaptic communication from RSC to M2 via corticocortical projection neurons in the PPC.

In thalamus, overlap of the anterogradely labeled RSC axons and retrogradely labeled M2-projecting thalamocortical neurons was observed in the anteromedial (AM) nucleus (Fig. 6*D*,*E*). Photostimulation of RSC axons evoked moderate to strong excitatory responses in most of these neurons (15 neurons recorded in 4 slices from $n = 4$ animals; Fig. 6*F*). In contrast, RSC input to M2-projecting neurons in the posterior nucleus (PO) was generally undetectable to weak (median RSC input to PO relative to median input to AM: 0.17, $p = 0.0078$, sign test, 15 AM and 9 PO neurons). These findings thus demonstrate a circuit-level basis for disynaptic cortico-thalamo-cortical communication from RSC to M2 via AM.

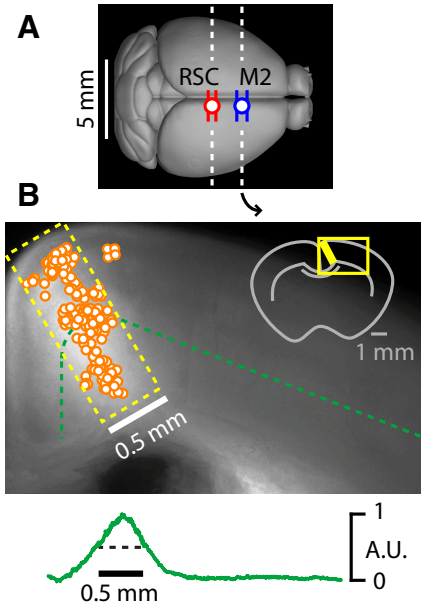

Figure 5. Anatomical locations of the RSC injections and M2 recordings. ***A***, Locations along the rostrocaudal axis of the RSC injections (red circle; mean ± SEM) and M2 slices (blue circle; mean ± SEM) used in the experiments. ***B***, Locations in the M2 slices of the recorded neurons (circles) are plotted on a median epifluorescence image of RSC axonal labeling in the M2. Bottom, Fluorescence intensity (plotted in arbitrary units, a.u.) along layer 5B (green dashed line in image).

M2 axons excite M2-projecting neurons in RSC

This study focused on the M2 side of the RSC→M2 circuit, but, because we found evidence for reciprocal innervation in the M2 (Figs. 1, 4), we also tested for reciprocal innervation on the RSC side. For this, we first examined the areal and laminar locations of M2-projecting neurons in RSC (Fig. 7). The RSC can be divided into multiple subareas based on cytoarchitechtonic structure and/or their long-range connectivity (for review, see Sugar et al. 2011). Here, we distinguished RSCg and RSCd regions based on bright-field microscopy and DAPI fluorescence (Fig. 7*A*). The corticopontine labeling pattern was used to define layer 5B neurons (Fig. 7*A*). To label M2-projecting neurons, we injected tracer in the M2 and prepared RSC slices (Fig. 7*B*,*C*). Epifluorescence imaging indicated that both of the RSC regions contained M2-projecting neurons, but with different laminar distributions: in the RSCd, M2-projecting neurons were primarily found in layers 2/3 and 5A (Fig. 7*D*); in the RSCg, M2-projecting neurons were present in layer 5A, but not in layer 2/3 (Fig. 7*E*).

←

(*Figure legend continued.*) versus RSC-projecting neurons in layer 6, the same injection scheme as in ***A*** was used, but with additional injection of retrograde tracer (Retrobeads) into thalamus (ventrolateral nucleus, VL). ***F***, Merged epifluorescence image of brain slices containing CT neurons (red) and RSC axons (yellow) in M2. ***G***, Example traces of RSC input recorded from neighboring CT neurons (red) and RSC-projecting neurons (blue) in M2 layer 6. ***H***, Group comparison of RSC input to CT and RSC-projecting neurons in layer 6 (not significantly different; see Results). ***I***, Schematic of the experimental paradigm: to compare RSC input to corticopontine-type PT neurons versus RSC-projecting neurons in layer 5B, the same injection scheme as in ***A*** was used, but with additional injection of retrograde tracer (Retrobeads) into the pons. ***J***, Merged epifluorescence image of brain slices containing corticopontine PT neurons (red) and RSC axons (yellow) in M2. ***K***, Example traces of RSC input recorded from neighboring corticopontine PT neurons (red) paired with layer 5B RSC-projecting neurons (blue) in M2. ***L***, Group comparison of RSC input to corticopontine PT and layer 5B RSC-projecting neurons (not significantly different; see Results). ***M***, Schematic of the experimental paradigm: to compare RSC input to corticocollicular-type PT neurons versus RSC-projecting neurons in layer 5B, the same injection scheme as in ***A*** was used, but with additional injection of retrograde tracer (Retrobeads) into superior colliculus (SC). ***N***, Merged epifluorescence image of brain slices containing corticocollicular PT neurons (red) and RSC axons (yellow) in M2. ***O***, Example traces of RSC input recorded from neighboring corticocollicular PT neurons (red) paired with layer 5B RSC-projecting neurons (blue) in M2. ***P***, Group comparison of RSC input to PT (corticocollicular) and layer 5B RSC-projecting neurons (not significantly different; see Results). ***Q***, Schematic of the experimental paradigm: to compare RSC input to corticocallosal IT neurons and RSC-projecting corticocortical neurons, same injection scheme as in ***A*** was used, but with additional injection of retrograde tracer (Retrobeads) into contralateral M2. ***R***, Merged epifluorescence image of brain slices containing corticocallosal IT neurons (red) and RSC axons (yellow) in M2. ***S***, Example traces of RSC input recorded from neighboring corticocallosal IT neurons (red) and RSC-projecting neurons (blue) in M2. ***T***, Group comparison of RSC input to corticocallosal IT neurons and RSC-projecting corticocortical neurons (not significantly different; see Results).

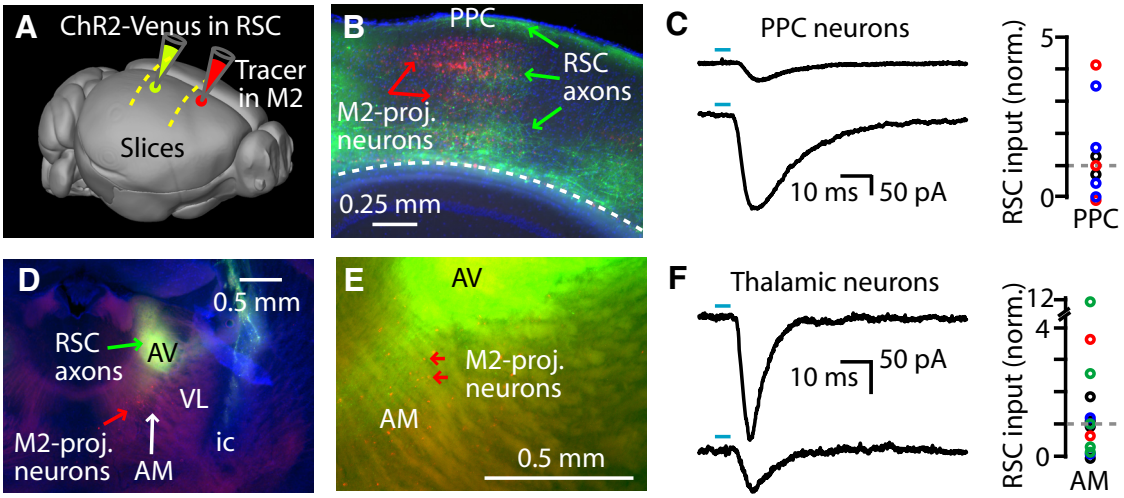

Figure 6. Disynaptic RSC connections to M2 via corticocortical and trans-thalamic circuits. ***A***, Injection strategy. AAV-ChR2-Venus was injected in the RSC to anterogradely label RSC efferent axons and retrograde tracer was injected in the M2 to label M2-projecting neurons. Coronal slices were then prepared and inspected to identify cortical and thalamic regions where RSC axons overlapped with M2-projecting neurons. ***B***, Epifluorescence image of a coronal slice containing the PPC showing anterogradely labeled RSC axons (green) and retrogradely labeled M2-projecting somata (red). Blue, DAPI staining. ***C***, Left, Example traces of RSC input recorded from M2-projecting neurons in layer 2/3 neurons of PPC in one animal. Right, Amplitudes of RSC inputs recorded from nine neurons normalized to the median value per animal (each color represents the set of neurons from one animal). ***D***, Epifluorescence image of the anterior thalamus showing anterogradely labeled RSC axons (green) in the anteroventral nucleus (AV) and retrogradely labeled M2-projecting somata in the AM nucleus (red). Blue, DAPI staining. ***E***, Higher-magnification epifluorescence image showing retrogradely labeled M2-projecting somata (red) in the AM, which partially overlap with anterogradely labeled RSC axons (green) projecting to contralateral thalamus. ***F***, Left, Example traces of RSC input recorded from M2-projecting neurons in AM in one animal recorded in relatively dorsal and mid locations in AM, as indicated. Right, Amplitudes of RSC inputs recorded from 15 neurons normalized to the median value per animal (each color represents the set of neurons from one animal).

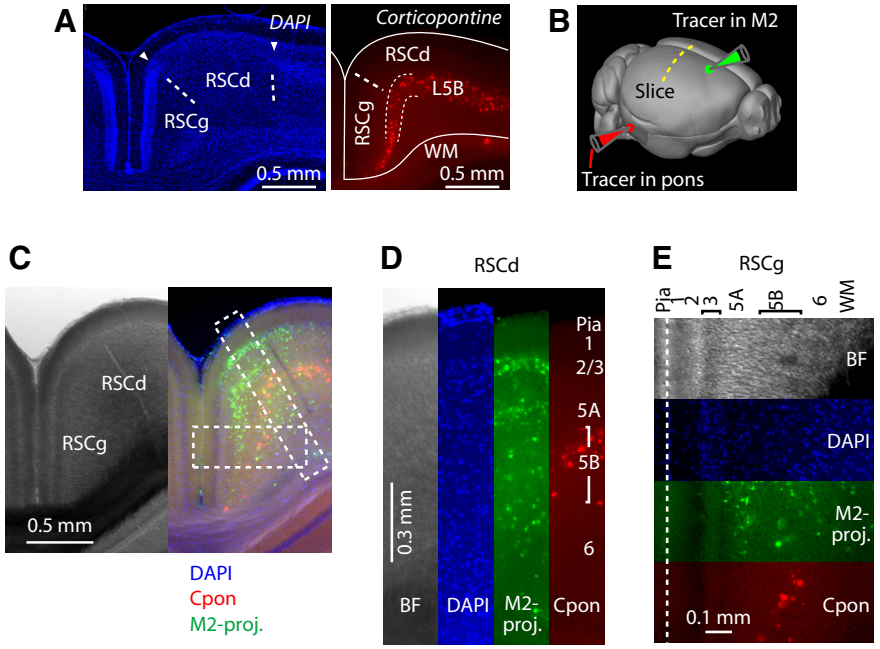

Figure 7. Areal and laminar distribution of M2-projecting neurons in RSC. ***A***, Left, DAPI stain showing differences in density of upper-layer neurons distinguishing the RSCg and RSCd areas of the RSC. Right, Retrograde labeling from the pons labels corticopontine neurons, the laminar distribution of which can be used to define layer 5B (L5B) in both the RSCd and RSCg. ***B***, Schematic of the experimental paradigm indicating injection of retrograde tracer (red Retrobeads) into the pons and retrograde tracer of another color (green Retrobeads) into the M2 to label corticopontine neurons and M2-projecting neurons in RSC, respectively. ***C***, Bright-field image (left) and merged epifluorescence image (right) of brain slice containing corticopontine (Cpon) and M2-projecting neurons in RSC. Blue, DAPI. ***D***, Labeling in RSCd, as indicated in ***C***. ***E***, Labeling in RSCg, as indicated in ***C***.

We first assessed the functional connections made by M2 axons onto RSC neurons by characterizing the laminar profile of input. We injected AAV-ChR2-Venus into M2 and prepared RSC slices (Fig. 8*A*). The M2 axonal labeling in these slices was strongest in RSCd, with less intense labeling in RSCg (Fig. 8*B*), so we focused on assessing input to RSCd neurons. Whole-cell recordings from radially aligned pyramidal neurons at different cortical depths in same slice (Fig. 8*C*) were analyzed to generate laminar profiles for the sets of neurons recorded in each slice (Fig. 8*D*). The input from M2 axons was stronger to layer 2/3 neurons than to neurons in deeper layers in the RSCd (Fig. 8*D*,*E*).

Because layer 2/3 of RSCd was also found to contain M2-projecting neurons in RSCd (Fig. 7*C*), we targeted recordings to these neurons to assess their innervation by M2 axons. We injected retrograde tracer and AAV-ChR2-Venus into the M2 and prepared RSC slices (Fig. 8*F*). Photostimulation of M2 axons evoked excitatory currents in M2-projecting neurons in RSCd (Fig. 8*G*). Consistent with the laminar profile (Fig. 8*E*), M2-projecting neurons in layer 2/3 received significantly stronger input than M2-projecting neurons in deeper layers (median ratio of layer 2/3 vs layer 5B responses: 3.39; $p = 0.02$, sign test; 7 layer 2/3 and 8 layer 5B neurons recorded in 5 slices from $n = 3$ animals, yielding 8 pairwise comparisons; Fig. 8*H*).

Therefore, these experiments investigating the RSC end of RSC–M2 circuits indicate an asymmetry reciprocity: unlike the M2 end, where the upper and lower layers (i.e., layers 2/3 and 5A/B) are both strong recipients of RSC input and also

both strong senders of outputs back to the RSC, at the RSC end, it is the layer 2/3 neurons of the RSCd that receive the strongest M2 inputs, but both layer 2/3 and layer 5A neurons send outputs to M2.

Discussion

The main finding in this study was that the RSC connects directly and extensively with the posterior M2. Cellular connectivity analyses revealed that RSC→M2 corticocortical projections comprise a matrix of monosynaptic excitatory connections innervating diverse types of projection neurons (Fig. 9). The postsynaptic targets of RSC axons in the M2 included neurons identified as projecting to multiple areas implicated in sensorimotor integration and motor control, such as the pontine nuclei and superior colliculus. This circuit organization implies a disynaptic influence of RSC activity on downstream activity in these divergent pathways. Also among the postsynaptic targets of RSC axons were RSC-projecting neurons, a finding that, together with the M2 input to M2-projecting neurons in the RSC, indicates that RSC and M2 form an interconnected reciprocal circuit.

Cellular connectivity in the RSC→M2 corticocortical circuit

RSC corticocortical axons excited M2 neurons in a distinct laminar profile. Neurons in all layers received RSC input, with relatively strong input to pyramidal neurons in middle and upper layers (2/3 through 5B), but weaker input to those in layer 6. Previous studies using similar methods have characterized laminar profiles for several other sources of long-range corticocortical and thalamocortical input to motor cortical areas in the mouse, each of which has distinct features (Mao et al., 2011; Hooks et al., 2013; Yamawaki et al., 2014; Suter and Shepherd, 2015; Yamawaki and Shepherd, 2015). For example, orbital cortex input to vibrissal M1 is relatively strong in layer 6 and weak in layers 2/3 through 5B (Hooks et al., 2013), inversely complementary to the laminar profile of RSC→M2 input observed here. The present findings reinforce the concept that multiple sources of long-range excitatory input converging on a cortical area collectively innervate neurons across all layers, with each upstream area contributing a subcircuit with a distinct source-specific laminar pattern (Hooks et al., 2013; Harris and Shepherd, 2015).

RSC inputs excited a wide spectrum of M2 projection neurons within and across layers. RSC axons innervated PT neurons in the M2 identified as corticopontine or corticocollicular neurons on the basis of retrograde labeling from the pons or superior colliculus, respectively. Previous studies in mouse motor cortical areas have shown that PT neurons receive excitatory input from several, but not all, long-range projections. For example, corticocortical axons from barrel cortex do not innervate PT neurons in vibrissal M1 (Mao et al., 2011) and thalamocortical axons from POm follow a similar laminar pattern of innervating only the upper layers (Hooks et al., 2013; Yamawaki et al., 2014). In contrast, corticocortical axons from rostral M2, S2, and contralateral MC all innervate layer 5B neurons, including PT neurons such as corticospinal neurons (Suter and Shepherd, 2015). In the RSC→M2 circuit characterized here, our findings suggest that the RSC, and thus the dorsal hippocampal system with which it is interconnected (Sugar et al., 2011), can access sensorimotor networks via monosynaptic connections to diverse types of PT neurons. These areas include brainstem precerebellar/cerebellar circuits (via corticopontine neurons) and midbrain motor-

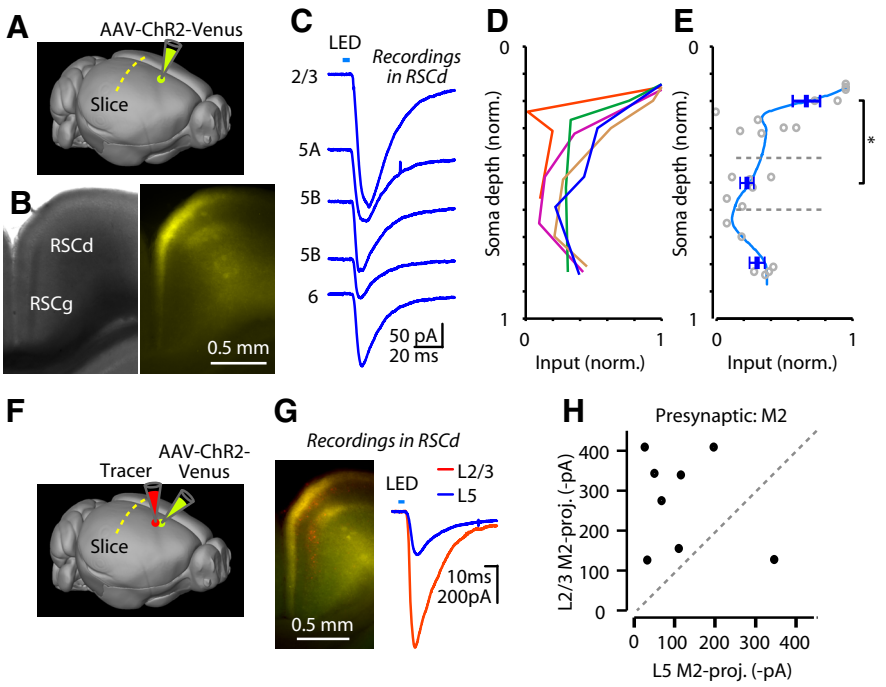

Figure 8. M2 axons excite M2-projecting neurons in RSC ***A***, Schematic of the experimental paradigm: AAV-ChR2-Venus was injected into the M2 to label M2 axons in RSC slices. ***B***, Bright-field image (left) and epifluorescence image (right) of brain slice containing M2 axons in RSC. ***C***, Example traces recorded from multiple neurons in the same RSC slice. ***D***, Laminar profiles from different slices. Blue trace is the profile for the responses in ***C***. ***E***, Same data as in ***D***, but grouped and averaged (top group, layer 2 through 5A; middle, layer 5B; bottom, layer 6). Rank-sum tests for the three groups (significance defined as $p < 0.05/3 = 0.0167$ to correct for multiple comparisons) showed the following: top versus middle: $p = 0.02$; middle versus bottom: $p = 0.06$; top versus bottom: $p = 0.48$. Blue lines indicate mean ± SEM for the data points in each group. Gray circles are same data as in ***D***, but unconnected by lines. ***F***, Schematic of the experimental paradigm indicating injection of retrograde tracer (retrobeads) and anterograde tracer (AAV-ChR2-Venus) into the M2 to label M2-projecting neurons and M2 axons in RSC. ***G***, Left, Merged epifluorescence image of M2-projecting neurons (red) and M2 axons (yellow). Right, Example traces of M2 input recorded from L2/3 or L5 M2-projecting neurons in RSC. ***H***, Group comparison of RSC input to L2/3 and L5B RSC-projecting neurons.

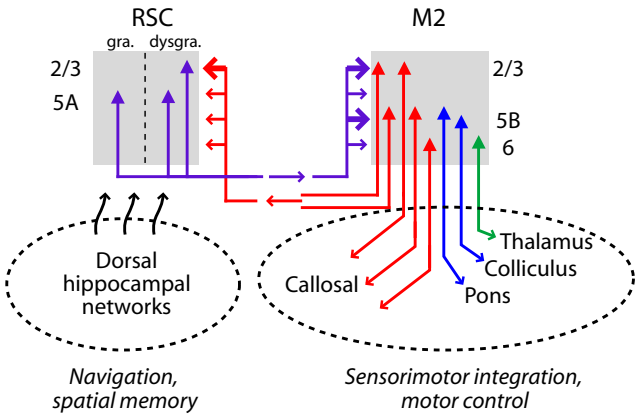

Figure 9. Schematic of RSC–M2 circuit. In the M2, the PT neurons are blue, IT red, and CT green. In the RSC, the M2-projecting neurons are purple.

related circuits involved in orienting reflexes (via corticocollicular neurons). RSC axons also innervated CT neurons in M2, suggesting disynaptic interactions of RSC with motor- and sensory-related thalamus via M2 (Hooks et al., 2013; Yamawaki and Shepherd, 2015) in addition to its direct interconnections with anterior thalamus.

IT neurons across all M2 layers were innervated by RSC axons, including neurons identified by retrograde labeling as RSC-projecting or callosally projecting corticocortical neurons. The finding of excitatory connectivity to RSC-projecting neurons indicates recurrent connectivity between RSC and M2, and thus a substrate for bidirectional communication between the two areas, whereas that of excitatory connectivity to callosally projecting neurons indicates a basis for engaging interhemispheric networks.

In addition to the monosynaptic connections forming a direct RSC→M2 circuit, we searched for disynaptic corticocortical connections via other cortical areas. We found that RSC axons projected to the PPC, where they excited M2-projecting corticocortical neurons, thus constituting a disynaptic corticocortical circuit (RSC→PPC→M2). In the rat, PPC similarly projects to a medial subregion of motor cortex medial to a zone innervated by S1 and S2 (Smith and Alloway, 2013; Ueta et al., 2013). In the mouse, S2 projections similarly target a lateral subregion of motor cortex, broadly innervating neurons across multiple layers and projection classes, including corticospinal neurons (Suter and Shepherd, 2015). Together, the previous results combined with our current findings suggests a medial-to-lateral topography of parietofrontal projections converging on motor cortex, with the RSC→M2 and RSC→PPC→M2 circuits among the most medial.

Using the same labeling strategy (anterograde ChR2 labeling in RSC and retrograde tracer injection in M2), we also searched for potential subcortical circuits mediating disynaptic communication between the two areas. We focused on thalamus both because thalamus is the main subcortical source of excitatory input to neocortex and because trans-thalamic circuits have been described in sensory cortical networks (Sherman, 2016). M2-projecting neurons in AM were found to receive input from RSC. These disynaptic corticocortical and trans-thalamic circuits suggest that communication between RSC and M2 occurs through multiple routes in addition to the monosynaptic RSC→M2 pathway. How these monosynaptic and disynaptic signals interact at the level of M2 remains to be investigated.

Functional implications and future directions

The main functional implication of our findings is that these RSC→M2 corticocortical connections provide a cellular basis for relaying information from dorsal hippocampal networks involved in spatial memory and navigation to neocortical networks involved in diverse aspects of sensorimotor integration and motor control. Goal-directed spatial navigation, an ethologically critical behavior, relies on landmark navigation and path integration and depends on a complex network of circuits (Taube, 2007; Aggleton and Nelson, 2015; Ito et al., 2015). The RSC is considered a key hub in the dorsal hippocampal system for collecting, processing, and expressing the context and self-motion related information involved in these processes (Epstein, 2008; Vann et al., 2009). Navigation, as well as other behaviors requiring action selection, also fundamentally requires action planning and execution and our study, by illuminating the cellular basis for RSC→M2 communication, suggests cellular mechanisms (circuit connections) linking cognitive and motor aspects of navigation. For example, we speculate that the direct excitation of corticocollicular and corticopontine projection neurons by RSC axons implies a role for these cellular pathways in coordinating ongoing activity in the sensorimotor system with that in the spatial orientation system during navigation. The M2→RSC reciprocal connectivity further suggests that the RSC also collects motor-related information from the M2. Given that M2 terminals innervate layer 2/3 of the RSCd, such information could potentially be used to coordinate spatial memory (Czajkowski et al., 2014) with spatial navigation.

In parallel with efforts to elucidate the functions of the RSC and M2 at the behavioral level, it will be important to understand the cellular and circuit-level mechanisms for synaptic integration and dynamic activity that mediate these functions. Whereas the present study focused on the RSC inputs to the M2, an important area for future studies is to better understand the cellular organization at the RSC end of this corticocortical pathway, including how specific types of RSC neurons integrate corticocortical input from M2 with the other types of inputs. Intriguingly, the other afferents to the RSC include an unusual long-range inhibitory projection from hippocampus (Jinno et al., 2007; Miyashita and Rockland, 2007) and an excitatory thalamocortical projection from the anterior nuclei that carries head direction signals to the RSC (Cho and Sharp, 2001; Winter et al., 2015). The cellular and subcellular targets of these inputs are largely unknown. The synaptic connections identified here, involving specific neuron classes amenable to genetic manipulation in the mouse, should provide a useful framework for further cellular-level studies of these circuits and their roles in behavior.

References

Aggleton JP (2014) Looking beyond the hippocampus: old and new neurological targets for understanding memory disorders. Proc Biol Sci 281: pii: 20140565. CrossRef Medline

Aggleton JP, Nelson AJ (2015) Why do lesions in the rodent anterior thalamic nuclei cause such severe spatial deficits? Neurosci Biobehav Rev 54:131–144. CrossRef Medline

Anderson CT, Sheets PL, Kiritani T, Shepherd GMG (2010) Sublayer-specific microcircuits of corticospinal and corticostriatal neurons in motor cortex. Nat Neurosci 13:739–744. CrossRef Medline

Brecht M, Krauss A, Muhammad S, Sinai-Esfahani L, Bellanca S, Margrie TW (2004) Organization of rat vibrissa motor cortex and adjacent areas according to cytoarchitectonics, microstimulation, and intracellular stimulation of identified cells. J Comp Neurol 479:360–373. CrossRef Medline

Cho J, Sharp PE (2001) Head direction, place, and movement correlates for cells in the rat retrosplenial cortex. Behav Neurosci 115:3–25. CrossRef Medline

Czajkowski R, Jayaprakash B, Wiltgen B, Rogerson T, Guzman-Karlsson MC, Barth AL, Trachtenberg JT, Silva AJ (2014) Encoding and storage of spatial information in the retrosplenial cortex. Proc Natl Acad Sci U S A 111:8661–8666. CrossRef Medline

Dong HW (2008) The Allen reference atlas. Hoboken, NY: Wiley.

Epstein RA (2008) Parahippocampal and retrosplenial contributions to human spatial navigation. Trends Cogn Sci 12:388–396. CrossRef Medline

Harris KD, Shepherd GMG (2015) The neocortical circuit: themes and variations. Nat Neurosci 18:170–181. CrossRef Medline

Hollis ER 2nd, Ishiko N, Yu T, Lu CC, Haimovich A, Tolentino K, Richman A, Tury A, Wang SH, Pessian M, Jo E, Kolodkin A, Zou Y (2016) Ryk controls remapping of motor cortex during functional recovery after spinal cord injury. Nat Neurosci 19:697–705. CrossRef Medline

Hooks BM, Hires SA, Zhang YX, Huber D, Petreanu L, Svoboda K, Shepherd GMG (2011) Laminar analysis of excitatory local circuits in vibrissal motor and sensory cortical areas. PLoS Biol 9:e1000572. CrossRef Medline

Hooks BM, Mao T, Gutnisky DA, Yamawaki N, Svoboda K, Shepherd GMG (2013) Organization of cortical and thalamic input to pyramidal neurons in mouse motor cortex. J Neurosci 33:748–760. CrossRef Medline

Ito HT, Zhang SJ, Witter MP, Moser EI, Moser MB (2015) A prefrontal-

thalamo-hippocampal circuit for goal-directed spatial navigation. Nature 522:50–55. CrossRef Medline

Jinno S, Klausberger T, Marton LF, Dalezios Y, Roberts JD, Fuentealba P, Bushong EA, Henze D, Buzsáki G, Somogyi P (2007) Neuronal diversity in GABAergic long-range projections from the hippocampus. J Neurosci 27:8790–8804. CrossRef Medline

Koike H, Demars MP, Short JA, Nabel EM, Akbarian S, Baxter MG, Morishita H (2016) Chemogenetic inactivation of dorsal anterior cingulate cortex neurons disrupts attentional behavior in mouse. Neuropsychopharmacology 41:1014–1023. CrossRef Medline

Komiyama T, Sato TR, O'Connor DH, Zhang YX, Huber D, Hooks BM, Gabitto M, Svoboda K (2010) Learning-related fine-scale specificity imaged in motor cortex circuits of behaving mice. Nature 464:1182–1186. CrossRef Medline

Li CX, Waters RS (1991) Organization of the mouse motor cortex studied by retrograde tracing and intracortical microstimulation (ICMS) mapping. Can J Neurol Sci 18:28–38. Medline

Little JP, Carter AG (2013) Synaptic mechanisms underlying strong reciprocal connectivity between the medial prefrontal cortex and basolateral amygdala. J Neurosci 33:15333–15342. CrossRef Medline

Mao T, Kusefoglu D, Hooks BM, Huber D, Petreanu L, Svoboda K (2011) Long-range neuronal circuits underlying the interaction between sensory and motor cortex. Neuron 72:111–123. CrossRef Medline

Miller AM, Vedder LC, Law LM, Smith DM (2014) Cues, context, and long-term memory: the role of the retrosplenial cortex in spatial cognition. Front Hum Neurosci 8:586. CrossRef Medline

Miyashita T, Rockland KS (2007) GABAergic projections from the hippocampus to the retrosplenial cortex in the rat. Eur J Neurosci 26: 1193–1204. CrossRef Medline

Oh SW et al. (2014) A mesoscale connectome of the mouse brain. Nature 508:207–214. CrossRef Medline

Passetti F, Chudasama Y, Robbins TW (2002) The frontal cortex of the rat and visual attentional performance: dissociable functions of distinct medial prefrontal subregions. Cereb Cortex 12:1254–1268. CrossRef Medline

Petreanu L, Huber D, Sobczyk A, Svoboda K (2007) Channelrhodopsin-2-assisted circuit mapping of long-range callosal projections. Nat Neurosci 10:663–668. CrossRef Medline

Petreanu L, Mao T, Sternson SM, Svoboda K (2009) The subcellular organization of neocortical excitatory connections. Nature 457:1142–1145. CrossRef Medline

Schoenenberger P, Schärer YP, Oertner TG (2011) Channelrhodopsin as a tool to investigate synaptic transmission and plasticity. Exp Physiol 96: 34–39. CrossRef Medline

Sherman SM (2016) Thalamus plays a central role in ongoing cortical functioning. Nat Neurosci 16:533–541. CrossRef Medline

Shibata H, Kondo S, Naito J (2004) Organization of retrosplenial cortical projections to the anterior cingulate, motor, and prefrontal cortices in the rat. Neurosci Res 49:1–11. CrossRef Medline

Smith JB, Alloway KD (2013) Rat whisker motor cortex is subdivided into sensory-input and motor-output areas. Front Neural Circuits 7:4. CrossRef Medline

Sugar J, Witter MP, van Strien NM, Cappaert NL (2011) The retrosplenial cortex: intrinsic connectivity and connections with the (para)hippocampal region in the rat: an interactive connectome. Front Neuroinform 5:7. CrossRef Medline

Suter BA, Shepherd GMG (2015) Reciprocal interareal connections to corticospinal neurons in mouse m1 and s2. J Neurosci 35:2959–2974. CrossRef Medline

Suter BA, O'Connor T, Iyer V, Petreanu LT, Hooks BM, Kiritani T, Svoboda K, Shepherd GMG (2010) Ephus: multipurpose data acquisition software for neuroscience experiments. Front Neural Circuits 4:100. CrossRef Medline

Tandon S, Kambi N, Jain N (2008) Overlapping representations of the neck and whiskers in the rat motor cortex revealed by mapping at different anaesthetic depths. Eur J Neurosci 27:228–237. Medline

Taube JS (2007) The head direction signal: origins and sensory-motor integration. Annu Rev Neurosci 30:181–207. CrossRef Medline

Tennant KA, Adkins DL, Donlan NA, Asay AL, Thomas N, Kleim JA, Jones TA (2011) The organization of the forelimb representation of the C57BL/6 mouse motor cortex as defined by intracortical microstimulation and cytoarchitecture. Cereb Cortex 21:865–876. CrossRef Medline

Ueta Y, Hirai Y, Otsuka T, Kawaguchi Y (2013) Direction- and distance-dependent interareal connectivity of pyramidal cell subpopulations in the rat frontal cortex. Front Neural Circuits 7:164. CrossRef Medline

Van Groen T, Wyss JM (2003) Connections of the retrosplenial granular b cortex in the rat. J Comp Neurol 463:249–263. CrossRef Medline

Vann SD, Aggleton JP, Maguire EA (2009) What does the retrosplenial cortex do? Nat Rev Neurosci 10:792–802. CrossRef Medline

Vélez-Fort M, Rousseau CV, Niedworok CJ, Wickersham IR, Rancz EA, Brown AP, Strom M, Margrie TW (2014) The stimulus selectivity and connectivity of layer six principal cells reveals cortical microcircuits underlying visual processing. Neuron 83:1431–1443. CrossRef Medline

Vogt BA, Miller MW (1983) Cortical connections between rat cingulate cortex and visual, motor, and postsubicular cortices. J Comp Neurol 216: 192–210. CrossRef Medline

Vogt BA, Paxinos G (2014) Cytoarchitecture of mouse and rat cingulate cortex with human homologies. Brain Struct Funct 219:185–192. CrossRef Medline

von Economo C (1929) The cytoarchitectonics of the human cerebral cortex. London: OUP.

Whitlock JR, Sutherland RJ, Witter MP, Moser MB, Moser EI (2008) Navigating from hippocampus to parietal cortex. Proc Natl Acad Sci U S A 105:14755–14762. CrossRef Medline

Winter SS, Clark BJ, Taube JS (2015) Spatial navigation. Disruption of the head direction cell network impairs the parahippocampal grid cell signal. Science 347:870–874. CrossRef Medline

Yamawaki N, Shepherd GMG (2015) Synaptic circuit organization of motor corticothalamic neurons. J Neurosci 35:2293–2307. CrossRef Medline

Yamawaki N, Borges K, Suter BA, Harris KD, Shepherd GMG (2014) A genuine layer 4 in motor cortex with prototypical synaptic circuit connectivity. eLife 3:e05422. CrossRef Medline

Yamawaki N, Suter BA, Wickersham IR, Shepherd GMG Combining optogenetics and electrophysiology to analyze projection neuron circuits. Cold Spring Harb Protoc, in press.